Energetics of elementary reaction steps relevant for CO oxidation: CO and O_2 adsorption on model Pd nanoparticles and Pd(111)

Matthias Peter, Sergey Adamovsky, Jose Manuel Flores Camacho and Swetlana Schauermann*

Received 2nd January 2013, Accepted 31st January 2013
DOI: 10.1039/c3fd00001j

The energetics of elementary surface processes relevant for CO oxidation, particularly CO and O_2 adsorption, were investigated by a direct calorimetric method on model Pd nanoparticles and on the extended Pd(111) single crystal surface. The focus of this study lies on a detailed understanding of how a nanometer scale confinement of matter affects the binding strength of gaseous adsorbates. We report adsorption energies and sticking coefficients of CO and O_2 measured as a function of the adsorbate surface coverage both on pristine and O-covered Pd surfaces. The reduced dimensions of the Pd substrate were found to affect the binding strength of the adsorbates in two principle ways: (i) *via* the change of the local adsorption environment that can result *e.g.* in stronger adsorbate bonding at the particle's low coordinated surface sites and (ii) *via* the contraction of the Pd lattice in small clusters and a concomitant weakening of chemisorptive interaction. Particularly for O_2 adsorption, the change of the adsorption site from a three-fold hollow on Pd(111) to the edge site on Pd nanoparticles (~4 nm sized on average) was found to result in a strong increase of the Pd–O bond strength. In contrast, CO adsorbs weaker on Pd nanoparticles as compared to the extended Pd(111) surface. In total, the binding energies of adsorbates on Pd and with this their surface coverages turn out to depend in a non-monotonic way on the particular structure of Pd surfaces, including the local structure of the adsorption site as well as the global properties of the small clusters arising *e.g.* from the lattice contraction.

I. Introduction

Confinement of matter at a nanoscopic scale is well known to result in new specific properties of a material. These new properties inherent to nanoparticles are particularly important for a number of practical applications of heterogeneous catalysis, such as *e.g.* CO oxidation over transition metals.[1,2] This reaction has attracted much attention in recent decades both in surface science and ambient pressure studies and many phenomena have already been well understood.[3–7] Despite the comprehensive understanding and general agreement on the microscopic mechanisms of CO oxidation over many transition metals, less information is available on the thermodynamics of the underlying surface processes. Particularly for metallic nanoparticles, the quantitative information on the adsorption and reaction enthalpies of elementary reaction steps, such as dissociative oxygen adsorption, CO adsorption on clean and oxygen-containing surfaces, CO and recombination

Department of Chemical Physics, Fritz-Haber-Institut der Max-Planck-Gesellschaft, Faradayweg 4-6, 14195 Berlin, Germany. E-mail: schauermann@fhi-berlin.mpg.de

with an adsorbed oxygen atom, is missing. It is a current scientific challenge to obtain detailed quantitative information on the binding strength of the gaseous adsorbates and on the reaction enthalpies as a function of the particle size and the particle surface composition, since these parameters essentially determine the surface coverages under the operation conditions and with this strongly affect the absolute reaction rates. The information would allow a deeper fundamental understanding of how the surface binds reactants and guides them through various elementary steps to the products, and provide a basis for a rational design of new catalytic and functional materials.

In previous studies related to CO oxidation, the energetics of surface processes were probed mainly by desorption-based methods such as temperature programmed desorption (TPD) and equilibrium adsorption isotherm measurements.[7–13] However, these methods can be applied correctly only for fully reversible adsorption–desorption processes such as *e.g.* CO adsorption and desorption on clean metals. In contrast, this condition does not apply for CO recombination with an oxygen atom or oxygen dissociative adsorption, which can be additionally accompanied by some side processes such as *e.g.* oxygen diffusion into the subsurface,[12–15] refacetting,[11,14] particle reconstruction,[7,16,17] as well as surface[17–19] and bulk oxide formation.[18,20] These obstacles and also the need for assumptions on the pre-exponential factors, which have to be made for the kinetic modeling of the desorption process, strongly limit the quantitative determination of binding and reaction energies related to CO oxidation by traditional desorption-based methods. A strategy to overcome these shortcomings is a direct calorimetric measurement of adsorption and reaction enthalpies under isothermal conditions.[21–24]

In this work, we report on the first direct calorimetric measurement of binding energies of gas phase molecules relevant to CO oxidation on model Pd nanoparticles and compare them to Pd(111) single crystal. The energetics of surface processes were probed on well-defined Pd nanoparticles supported on a thin Fe_3O_4 crystalline oxide film prepared *in situ* under ultra-high vacuum (UHV) conditions. We apply a recently developed UHV single crystal adsorption calorimeter (SCAC) based on molecular beam techniques[24] to investigate the energetics of dissociative oxygen adsorption and CO adsorption on clean and O-precovered Pd nanoparticles and on Pd(111), as a reference. With this approach we address the question: how do the reduced dimensions of a metallic substrate (extended laterally stiff single crystal *vs.* small atomically flexible nanoparticles) and its surface composition affect the adsorption strength of the reactive species?

II. Experimental procedure

The adsorption experiments were performed at the Fritz-Haber-Institute (Berlin) in an ultra-high vacuum (UHV) single crystal adsorption calorimetry (SCAC) apparatus based on molecular beam techniques described in detail elsewhere.[24] An effusive doubly differentially pumped multi-channel array source was employed to produce an oxygen (Linde, purity 99.999%) beam at the intensity 1×10^{14} molecules cm^{-2} s^{-1} (5.3×10^{-7} mbar on the sample surface) or CO beam (Linde, purity 99.995%) at the intensity 1×10^{14} molecules cm^{-2} s^{-1} (5.3×10^{-7} mbar on the sample surface). The beam was cut into pulses of 266 ms length by a remote-controlled chopper, after that the gas impinged on a sample prepared on an ultrathin (1 μm) single crystal (Pd(111) or model supported catalysts grown on Pt(111)). The small change in the temperature of the sample caused by adsorption of oxygen was measured by a heat detector, consisting of a 9 μm-thick β-polyvinylidene fluoride (β-PVDF) pyroelectric ribbon coated with Au on both sides. The energy calibration was performed by applying pulses of laser light (HeNe, Linos, wavelength 632.8 nm, 5 mW), which passes through the same path as the molecular beam and is chopped in a way identical to the molecular flux. Simultaneously, the fraction of the molecules adsorbed in a single beam pulse (*i.e.*, the sticking coefficient) was defined by the

modified King–Wells method[25] with a quadrupole mass spectrometer (QMS Hiden, HAL 301/3F) in a non-line-of-sight geometry.

The $Pd/Fe_3O_4/Pt(111)$ model catalyst was prepared by growing a thin (~50 Å) $Fe_3O_4(111)$ film on a Pt(111) single crystal by repeated cycles of Fe (>99.99%, Goodfellow) physical vapor deposition at a substrate temperature of ~120 K and subsequent oxidation at 875 K (see refs. 26 and 27 for details). The cleanliness and the quality of the oxide film were checked by AES and LEED. Pd particles were grown *in situ* by physical vapor deposition from a Pd rod (Goodfellow, >99.9%) using a commercial evaporator (Focus, EFM 3) with a deposition rate of 0.3 Å min^{-1} (2.04×10^{14} atoms cm^{-2} min^{-1}). The nominal deposition thickness value amounts to 4.0 Å, or to 2.8×10^{15} atoms cm^{-2}. Directly after Pd deposition, the sample was annealed to 600 K and cooled to 300 K, and a microcalorimetric measurement of oxygen or CO adsorption heats was performed. The evaporation rates of Fe and Pd were calibrated by a quartz-crystal microbalance (QCM, Sigma instruments).

III. Results and discussion

III.A Combined energy and sticking coefficient measurement: CO adsorption on supported Pd nanoparticles and Pd(111)

The model surface employed in this study consisted of Pd nanoparticles supported on a well-ordered thin Fe_3O_4 film grown on a Pt(111) single crystal (Fig. 1; for details of the preparation procedure and structural characterization by scanning tunneling microscopy (STM) see refs. 26 and 27). On average, a Pd particle on this surface is about 4 nm in diameter and contains ~720 Pd atoms; the particle density on the support amounts to 3.8×10^{12} particles cm^{-2}. According to STM data, the particles are crystalline and exhibit a nearly hexagonal shape with a flat top facet, which indicates that the particles grow in (111) orientation and their sides are terminated with (111) and (100) facets.

In the calorimetric experiment, two parameters were measured simultaneously and independently: the sticking coefficient and the corresponding adsorption energy (differential adsorption heat). The details of the calorimetric measurement were comprehensively discussed elsewhere.[24] Briefly, we prepare a model catalyst on an ultrathin (1 μm) Pt(111) single crystal and transfer it *in situ* to the calorimeter. In

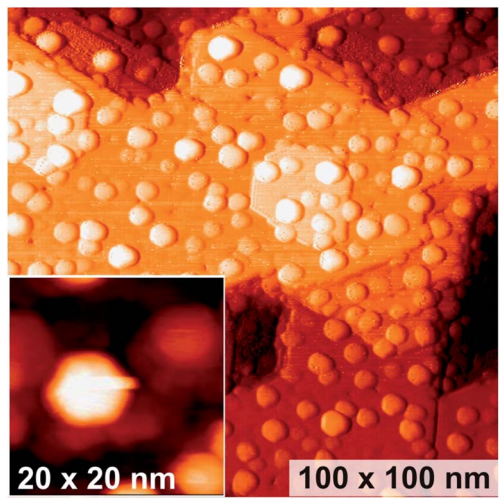

Fig. 1 STM image of the $Pd/Fe_3O_4/Pt(111)$ model catalyst used in this study, nominal Pd deposition thickness 4 Å, from ref. 27.

a calorimetric experiment a pulse of gas from a chopped molecular beam impinges on an ultrathin single crystal surface. A fraction of the molecules striking the surface adsorb and this heat input causes a transient temperature rise (~10 mK), which is measured by a pyroelectric heat detector. The absolute energy calibration is performed by applying pulses of laser light of known energy, which passes through the molecular beam and is chopped in a way identical to the molecular flux. Two parameters, critically influencing the calibration – the absolute power of the laser light and the reflectivity of the sample – are measured *in situ*. Simultaneously, the absolute fraction of the molecules adsorbed in a single beam pulse is measured in a sticking coefficient measurement by the King–Wells method[25] in order to determine the absolute value of deposited energy per number of adsorbed molecules.

Fig. 2 shows the complete calorimetric data set obtained at 300 K: the sticking coefficients (Fig. 2a and 2b) and the differential adsorption heats (Fig. 2c and 2d) plotted as a function of CO surface coverage for Pd nanoparticles and Pd(111) single crystal. Note that at this temperature CO does not permanently chemisorb on the Fe_3O_4 support[28] but on the Pd particles only and the experimental time scale is long enough in order to let the molecules diffuse over the surface and find the strongest adsorption site.[29]

The initial CO sticking coefficient on Pd(111) (Fig. 2b) reaches the value 0.72 ± 0.03 and remains nearly constant until the CO surface coverage of $\sim 2.7 \times 10^{14}$ CO molecules cm^{-2} (or 0.18 CO molecules per surface Pd atom) is achieved. After that it decreases to a quasi steady state value[21] of about 0.3 for a CO coverage of 0.76×10^{15} molecules cm^{-2} (or 0.5 CO molecules per surface Pd atom) in saturation. The apparent non-zero sticking coefficient close to saturation arises from the partial CO desorption between the beam pulses and additional adsorption of CO when the next pulse hits the surface (see full discussion in refs. 21,23,24). The CO saturation coverage on Pd(111) is in excellent agreement with the previously reported value 0.5 with reference to the number of surface Pd atoms, which was obtained by a number of independent surface-sensitive techniques (see *e.g.* refs. 30–33). The value of the initial sticking coefficient measured in this study is somewhat lower than the previously reported values of 0.8–1.0[34] and 0.95 ± 0.05.[35] Qualitatively similar dependence of the sticking coefficient on surface CO coverage was observed on Pd

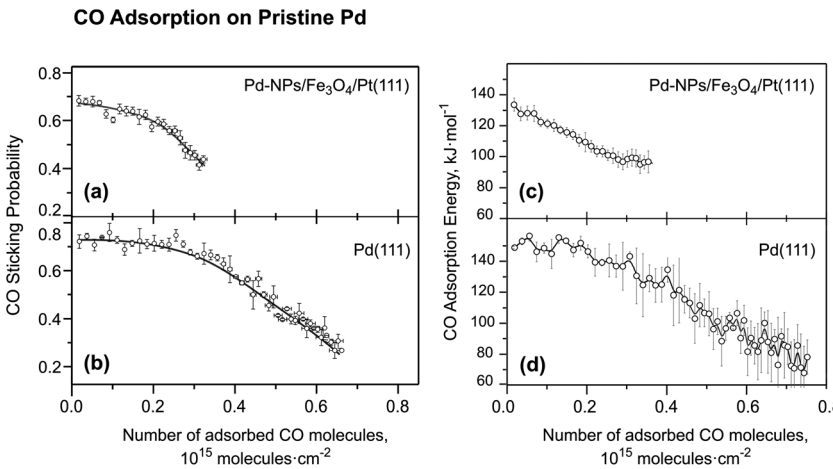

Fig. 2 Sticking probability plotted as a function of number of adsorbed CO molecules for Pd nanoparticles (a) and for Pd(111) (b). Differential heats of adsorption plotted as a function of number of adsorbed CO molecules for Pd nanoparticles (c) and Pd(111) (d). All data were obtained at 300 K. The data are shown as an average of four to six independent measurements on freshly prepared surfaces. The error bars correspond to the error of the mean.

nanoparticles, with the initial sticking coefficient amounting to 0.68 ± 0.02 and the saturation coverage of 0.4 × 10^{15} molecules cm^{-2} (Fig. 2a). The final CO surface coverage expressed as a number of adsorbed CO molecules per surface Pd atom is ~0.48, which is in good agreement with the value 0.5 measured on Pd(111)[30–33] and Pd(100)[36] single crystal surfaces at room temperature. This result shows that the absolute adsorption capacity of investigated Pd nanoparticles is close to that of the single crystal surfaces and indicates that no dramatic changes in the adsorption mechanism occur upon reduction of the particle sizes down to 4 nm. It is apparent that the general adsorption mechanism follows a typical precursor type behavior, which was previously observed on the Pd single crystal surfaces (compare *e.g.* refs .34 and 35).

The sticking coefficient data can be rationalized on a basis of the so-called "capture zone" effect.[37–41] This phenomenon is based on the existence of two adsorption channels: the adsorbate molecules can either directly impinge on the metal particles and chemisorb or they can be trapped in a weakly bound state on the support and reach the particles *via* surface diffusion. The capture zone is defined as an area from which impinging adsorbates can be collected by the particles. This effect was predicted and later experimentally confirmed to considerably enhance the adsorption rate on the particles.[5,7] In the present experiments, the capture zone effect was found to play an important role in the overall adsorption rate. The magnitude of this effect can be evaluated from the comparison of the measured initial sticking probability data on the supported particles and the estimate of the highest possible initial sticking probability on the particles of the same size in absence of the contribution from the support. For the Pd particles investigated in this study (average particle size of ~4 nm and the island density 3.8 × 10^{12} particles cm^{-2}), about 48% of the Fe_3O_4 surface area is covered by Pd particles. This means that only ~48% of the impinging molecules arrive directly on the metal surface and about 52% interact first with the support. If one assumes the highest possible sticking coefficient on metallic Pd to be 1.0 and fully neglects the contribution from the capture zone effect, an initial sticking coefficient close to 0.48 can be expected (corresponding to the scenario when 48% of the molecules completely stick to the metal particles). However, the experimentally measured initial sticking coefficient 0.68 is a factor of 1.4 higher than the estimated upper limit for the direct sticking on the metal particles. This observation can be rationalized only in the scope of the "capture zone" model, where the additional 20% of the impinging molecules become first weakly trapped on the support and reach the Pd particles, where they strongly chemisorb, within their residence time. Thus, the capture zone effect leads to an enhancement of the adsorption rate by a factor of at least 1.4. If one assumes the experimentally measured value of the sticking coefficient 0.74 on Pd(111), the enhancement factor increases to ~1.9. Note that CO does not chemisorb on Fe_3O_4 at the experimental temperature of 300 K,[28] so that the enhanced adsorption cannot be explained simply by CO chemisorption on the support. Similar enhancement of the initial sticking probability due to the "capture zone effect" has been reported for a number of model surfaces consisting of Pd nanoparticles supported on various oxides.[26,40,41]

The differential adsorption heats obtained on Pd nanoparticles and Pd(111) are plotted as a function of CO surface coverage in Fig. 2c and 2d. Each curve is an average of 4 to 6 independent measurements on freshly prepared model systems. On Pd(111), the heat of CO adsorption initially amounts to 149 ± 4 kJ mol^{-1}. After adsorption of about 0.76 × 10^{15} CO molecules cm^{-2} the surface of the particles reaches saturation (with the corresponding CO surface coverage of 0.5 ML with respect to the number of surface Pd atoms) and the adsorption heat decreases to the final non-zero value 75 ± 9 kJ mol^{-1}, which is related to the adsorption–desorption equilibrium established in quasi steady state regime.[21] Note that the final heat value is subject to large statistical errors since a very small absolute number of CO molecules is added in a single CO pulse, which is difficult to measure. Two reasons can account for the decreasing adsorption energy with growing CO coverage: intermolecular

repulsion of neighboring CO molecules and increasing competition for the d-electrons of Pd nanoclusters participating in the CO–Pd bonding. For the Pd(111) single crystal surface, both the initial heat of adsorption as well as the saturation coverage at 300 K were found to be in a very good quantitative agreement with the data reported earlier in the literature.[42–45]

A qualitatively similar dependence of the adsorption heat on CO coverage was observed for Pd nanoparticles. On this surface, the initially high adsorption heat 134 ± 4 kJ mol^{-1} continuously decreases with growing CO coverage and reaches a lower steady state value $\sim$90 kJ mol^{-1} after adsorption of $\sim 0.4 \times 10^{15}$ molecules cm^{-2}. Remarkably, the initial adsorption energy is 15 kJ mol^{-1} lower than the corresponding value on the Pd(111) surface despite the fact that Pd nanoparticles contain a large fraction of low-coordinated surface sites, such as edges and corners, which are often discussed to be strong binding sites. Previously, we comprehensively investigated the dependence of the CO initial adsorption energy on Pd as a function of the cluster size in the broader size range from 2 to 8 nm (or from 120 to 4900 Pd atoms per particle).[46] The initial adsorption heats were compared in the lowest coverage limit, where the adsorption heat is determined by the interaction of individual CO molecules with metal, and is not perturbed by the CO intermolecular repulsion or by the competition for the d-electrons. In the whole investigated size region the adsorption heat was observed to strongly decrease with decreasing particle size: from 126 ± 3 kJ mol^{-1} on 8 nm-sized Pd particles to 106 ± 1 kJ mol^{-1} on the smallest $\sim$2 nm clusters. Additionally, all investigated particles showed smaller initial adsorption heat as compared to the single crystal surface (149 ± 3 kJ mol^{-1}).

It has to be pointed out that the surface of the Pd particles investigated in this work exposes mainly (111) terraces along with a smaller fraction of (100) facets and low-coordinated defect sites such as edges and corners. According to theoretical calculations, such irregular sites exhibit higher CO adsorption energies than Pd(111).[47] Experimentally, there is a general agreement that the CO adsorption energy on the (100) plane is about 10–15 kJ mol^{-1} higher than on the (111) plane (see *e.g.* ref. 42). However, the dramatic effect of low-coordination defect sites (like step edges) on the CO adsorption energy, such as observed for Pt(111),[48] is *not* seen on Pd(111).[42,44] Ramsier, Lee and Yates[44] even concluded from comparing CO TPD and adsorption energies for different stepped Pd facets that "structure of the Pd surface is only of minor importance in CO adsorption/desorption kinetics." These experimental results suggest that the degree of coordination of the Pd surface atoms on the stepped surfaces is not as important in determining the CO adsorption energy as on surfaces of other metals like Pt. Therefore, the increasing fraction of low-coordination Pd atoms with decreasing particle size may not be the dominant effect in determining how the CO adsorption energy varies with Pd particle size. Instead, other size-dependent properties of a Pd nanocluster have to be responsible for the obtained decrease of the initial adsorption enthalpy of carbon monoxide with decreasing the particle size.

First, the decrease of the chemisorption energy on Pd nanoparticles can result from the contraction of the lattice parameter of a small metal nanoparticle. Previously, it has been demonstrated experimentally[49,50] that the interatomic bond length in small metal particles decreases with decreasing particle size. It is now well established also by computational studies of various metals including Pd[51–53] that relaxed structures of metal clusters exhibit shorter interatomic distances than bulk crystals. This phenomenon has been rationalized as a result of decreasing average coordination number of the atoms with the higher surface-to-volume ratio of the cluster.[51–53] Particularly for Pd, it was shown that the average calculated Pd–Pd nearest-neighbor distance decreases linearly with decreasing linear dimension of a nanoparticle in the range of 55–260 atoms per cluster.[54] This lattice contraction in the small metal clusters was theoretically shown to result in a reduction of the adsorbate binding energy. Particularly for CO adsorption on the Pd clusters consisting of 55–260 atoms, it was demonstrated that the clusters with optimized structures show systematically lower

adsorption energies by about 10–15 kJ mol^{-1} than the clusters with a bulk terminated geometry, *i.e.* with all interatomic distances d(Pd–Pd) = 275 pm.[55] This finding agrees with the principle of bond order conservation:[56,57] in the contracted clusters, one expects weaker adsorption bonds and stronger binding within the adsorbate as a result of better saturated valences of the substrate atoms. The decrease of the adsorbate binding energy with the lattice constant can be also rationalized in terms of the strain effect, which is associated with a downward shift of the valance d-band with decreasing lattice parameter.[55,58] Such effects were found not to be restricted to 3-fold hollow sites on (111) facets, but reflect a general trend that also holds for adsorption at other sites of the particles such as bridge sites and edges.[55]

A second reason for the decrease of adsorption heat of a gas-phase molecule on the small metal clusters is a feasible weakening of the dispersion force (van der Waals interaction) that is induced by dynamic response of bulk electrons of the metal to charge density fluctuations in an adsorbed molecule. Previously, it has been shown that the electron population at the Fermi edge, which is mainly relevant for this interaction, drastically changes with the cluster size in the range of a few nanometers.[59] The gradual decrease of the initial adsorption heat with the decreasing cluster size can be reasonably understood, since smaller clusters contain less electrons available for dynamic response. Similar behavior has been previously observed in TPD studies for methane on Pd[60] and NO on Ag nanoclusters[61] and was also attributed to the reduced polarizability of the small metal nanoparticles.

III.B Combined energy and sticking coefficient measurement: O_2 dissociative adsorption on supported Pd nanoparticles and Pd(111)

Dissociative oxygen adsorption was investigated on the same two Pd surfaces at 300 K, at which oxygen adsorbs dissociatively and does not stick to the oxide support. Fig. 3 shows the obtained sticking coefficients (Fig. 3a and 3b) and the adsorption energies (Fig. 3c and 3d) plotted as a function of O surface coverage.

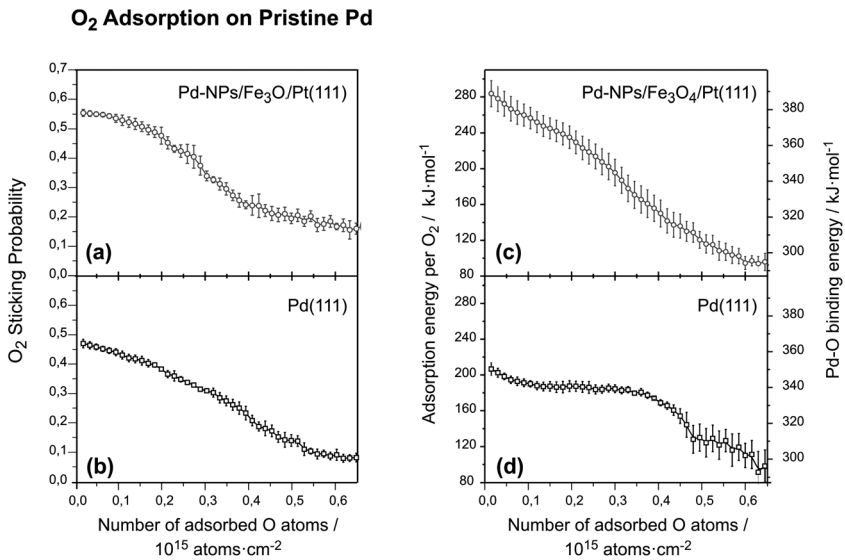

Fig. 3 Sticking probability of oxygen plotted as a function of number of adsorbed O atoms for Pd nanoparticles (a) and for Pd(111) (b). Differential adsorption heat per mole of O_2 (left axis) and Pd–O binding energy (right axis) plotted as a function of the number of adsorbed O atoms. The sticking coefficients and adsorption heats were obtained at 300 K and are shown as an average of four to six independent measurements on freshly prepared surfaces. The error bars correspond to the error of the mean.

On Pd(111), the initial O_2 sticking probability reaches 0.47 ± 0.01 and steadily decreases until the O surface coverage approaches the value of $\sim 0.5 \times 10^{15}$ O atoms cm^{-2} (or $\sim$0.3 O atoms per surface Pd atom, Fig. 3b). The measured saturation coverage is in agreement with the literature data ranging from 0.25 to 0.4 observed for different O_2 exposures on this surface.[9,10,12,13,15] Previously, formation of O coverages larger than 0.25 was observed for high O_2 exposures and a number of reasons were suggested to be responsible for this phenomenon, such as *e.g.* slow formation of compressed O overlayers or O diffusion into the subsurface region.[12–15] Apparently, similar processes might take place also under our reaction conditions and they appear to be more pronounced on Pd nanoparticles. The detailed analysis of oxygen adsorption in the high coverage regime both on Pd(111) and Pd nanoparticles will be the subject of a forthcoming publication.[62] Here, we will mainly focus on oxygen coverages up to 0.25, at which these side processes do not play any significant role.

On Pd nanoparticles, a qualitatively similar dependence of the sticking coefficient on surface O coverage was observed, with the initial sticking coefficient amounting to 0.55 ± 0.01 and the saturation coverage lying between 0.4×10^{15} and 0.5×10^{15} O atoms cm^{-2} (Fig. 3a). Note that the initial sticking coefficient of O_2 on the Pd clusters is even higher than on Pd(111) despite the fact that only $\sim$48% of the surface is covered by Pd. To rationalize this high dissociative sticking coefficient, we estimated the capture zone effects on this surface. If one assumes the same value of the initial sticking coefficient as on Pd(111) (0.47), the fraction of the molecules that impinge directly on the Pd nanoparticles and remain adsorbed amounts to 0.23. The rest of the adsorbed molecules (relative fraction $\sim$0.32) must first be trapped on the Fe_3O_4 support and then diffuse to the metal particles within their residence time and dissociate on it (note that O_2 neither dissociatively nor molecularly adsorbs on the oxide support under our reaction conditions). This scenario does not seem to be very likely though, since it implies that a molecule impinging on the surface has a higher probability to be trapped on the Fe_3O_4 support and then undergo the dissociative adsorption on Pd particles than directly stick and dissociate on metallic nanoparticles (0.62 *vs.* 0.47, correspondingly). More realistically, O_2 molecules have higher initial probability to dissociate on Pd nanoparticles than on Pd(111) as the first type of surface contains a large number of potentially highly reactive low-coordinated adsorption sites. To evaluate the feasibility of this hypothesis, we estimated the magnitude of the capture zone effect for the boundary case when the initial sticking coefficient of O_2 on Pd nanoparticles is equal to unity. In this case, the fraction of the molecules impinging directly on the particles and dissociating there should amount to 0.48 and only the remaining fraction of O_2 amounting to 0.07 has to arrive from the support and dissociate on the metal, which might be a realistic scenario. Based on the available data set, the exact quantification of the initial sticking coefficient on Pd nanoparticles is not possible, since the experimentally measured value is a convolution of the intrinsic initial sticking coefficient with the capture zone effects. The strategy to tackle this problem would be *e.g.* a systematic variation of the particles sizes and density on the support, thus allowing an estimation of the relative contribution of the capture zone effect. The corresponding experiments are currently under way. Based on the available data, we can only conclude that the intrinsic initial sticking coefficient on Pd nanoparticles lies in the range between 0.47 and 1.0.

Fig. 3c and 3d show the dependence of the differential O_2 adsorption heat (left axis) and the calculated Pd–O bonding strength (right axis) plotted as a function of O atoms surface coverage for Pd nanoparticles and Pd(111).

Both model surfaces show a very strong coverage dependence of oxygen binding energies. For Pd(111), the initial adsorption energy on the clean surface amounts to $\sim 205 \pm 7$ kJ mol^{-1}, which drops to about 100 kJ mol^{-1} close to saturation. As discussed above, two reasons might potentially account for the decreasing adsorption energy with increasing O coverage: interatomic repulsion of neighboring O atoms, and increasing competition for the d-electrons of Pd atoms participating in the O–Pd bonding. A qualitatively similar dependence of the adsorption energy on the O

coverage was observed for Pd nanoparticles. However, there is a very pronounced difference in the initial adsorption energy between the Pd clusters and Pd(111). While O binds with ~205 kJ mol^{-1} on the pristine Pd(111) surface, the initial binding energy rises to ~280 ± 13 kJ mol^{-1} on the pristine Pd nanoparticles (both values are differential adsorption heats for O_2 molecule). Note that on average only about 7 O atoms per Pd nanoparticle (comprising ~320 surface Pd atoms) contribute to the measured initial adsorption energy, which allows us to consider this energy value as a limiting case for the interaction of an individual O atom with a pristine Pd nanoparticle. Also note that neither subsurface O diffusion nor surface oxide formation can occur at the experimental low temperature conditions (300 K) and low oxygen coverages, which could otherwise affect the measured values.

The energy value obtained by SCAC for Pd(111) in the lowest coverage limit (205 kJ mol^{-1} at the surface coverage 0.01×10^{15} O atoms cm^{-2}) is in good agreement with literature values of O adsorption energies at low coverages situated in the range of 210 to 230 kJ mol^{-1}.[10,13,15] In contrast, the very high initial energy value obtained for Pd nanoparticles (275 kJ mol^{-1} at 0.01×10^{15} O atoms cm^{-2}) cannot be compared to any value reported in TPD studies either for low Miller index Pd surfaces, or for stepped Pd crystals, which typically span the range between 190 and 230 kJ mol^{-1}.[9,13,15,63] Thus, this high initial adsorption energy must be related to some structural feature inherent to Pd nanoparticles, which cannot be reproduced even by the steps of the high Miller index Pd surfaces. Such adsorption sites on Pd nanoparticles might be the low coordinated surface sites such as particle edges and corners. In previous STM studies on supported Pd nanoparticles, oxygen was shown to modify such sites first, indicating thus that they are the strongest adsorption sites on a Pd nanoparticle.[64] To check the feasibility of this explanation, we carried out CO titration experiments by infrared reflection absorption spectroscopy (IRAS) to identify the preferential adsorption sites of oxygen on Pd nanoparticles. In previous IRAS studies, the CO molecule was shown to be a suitable probe molecule for probing different adsorption sites on Pd nanoparticles, allowing independent identification of the regular adsorption sites on the (111) terraces and the low-coordinated adsorption sites such as edges and corners.[65] With this spectroscopic approach, it was experimentally confirmed that oxygen adsorption first modifies the low coordinated surface sites such as edges and corners. For more details, the reader is referred to ref. 66. From these observations we can unambiguously attribute the unexpectedly high initial adsorption energy (280 kJ mol^{-1}), measured in a calorimetric experiment on supported Pd nanoparticles, to oxygen adsorption at edge and corner sites. It remains, however, an open question as to why the edge sites of Pd nanoclusters interact so strongly with adsorbed oxygen. Further theoretical work is needed in order to rationalize the microscopic nature of this phenomenon, which can presumably originate from the reconstruction or refaceting of the particles edges that was previously reported in the literature.[64,67] It is also feasible that the edge sites exhibit a higher activity in dissociating of O_2 molecules, which can account for the experimentally observed high values of the initial sticking coefficient on Pd nanoparticles.

III.C CO adsorption on supported Pd nanoparticles and Pd(111) precovered by O

Under the reaction conditions, both CO and oxygen interact with the surface, which is partially or nearly fully covered by co-reactants. The presence of co-adsorbates can significantly change the binding energies and consequently strongly affect the surface coverages under the operation conditions. For the reactions involving a dissociative step, such as CO oxidation, even small changes in the surface coverage might result in switching to a "poisoning" regime, where high concentration of one reactant (CO) can nearly completely suppress dissociation of the other one (O_2).[5,7] Therefore it is a very important issue and a current scientific challenge to accurately determine the binding energies in the systems of two co-adsorbates and understand how this binding strength depends on the structure of the underlying metal

substrate. To approach this goal, we measured the binding energies of CO on both Pd surfaces pre-saturated with oxygen. Oxygen deposition was carried out at 300 K to enable dissociation of molecular species, and immediately afterwards CO adsorption energies were measured at 100 K, at which CO does not react with O to produce CO_2.

The results of these experiments are displayed in Fig. 4a and 4b for Pd nanoparticles and Pd(111), respectively. They show that both surfaces precovered with oxygen exhibit similar adsorption capacity for CO to the clean Pd surfaces. The measured saturation values are $\sim 0.75 \times 10^{15}$ molecules cm^{-2} on Pd(111) and $\sim 0.50 \times 10^{15}$ molecules cm^{-2} on O/Pd nanoparticles (compare to the values 0.76×10^{15} molecules cm^{-2} and 0.4×10^{15} molecules cm^{-2} on clean Pd surfaces, correspondingly). However, it should be noted that CO adsorption on the clean surfaces was investigated at 300 K, while the experiments on the O-precovered surfaces were carried out at 100 K to avoid surface reaction between adsorbed CO and O. According to previous experimental and theoretical studies on Pd(111), CO occupies two hollow sites (hcp and fcc) at 300 K forming a $c(2 \times 4)_{2CO}$ overlayer with the saturation coverage of 0.5 CO molecules per surface Pd atom.[68,69] At 100 K, the CO saturation coverage increases on the clean Pd(111) surface to 0.75 due to occupation of an additional on-top adsorption site per unit cell.[70,71] On Pd(111) precovered with oxygen, CO forms a new mixed $p(2 \times 2)_{CO+O}$ phase in the temperature range 60–110 K.[72] STM results in combination with DFT calculations suggest that this overlayer structure is consistent with the occupation of a (fcc) hollow site by one oxygen

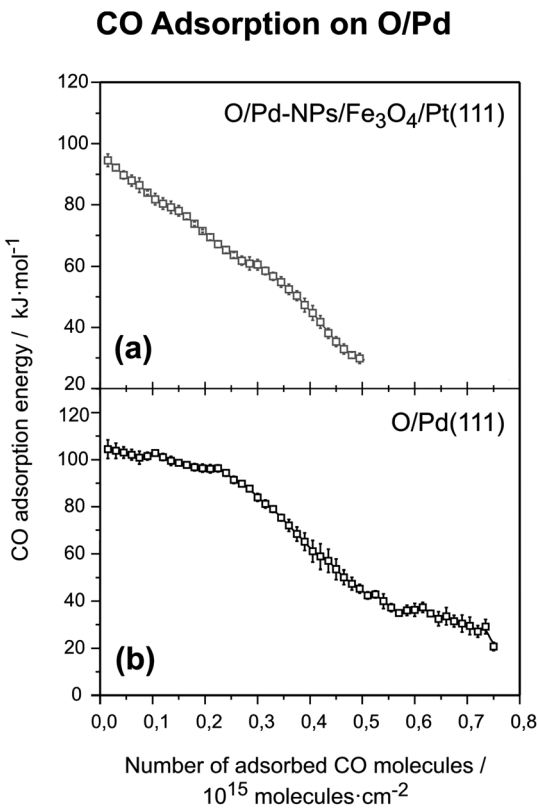

Fig. 4 Differential heats of CO adsorption plotted as a function of number of adsorbed CO molecules for Pd nanoparticles (a) and Pd(111) (b) pre-covered with a monolayer of O atoms. Oxygen was deposited at 300 K, CO adsorption experiments were carried out at 100 K.

atom per unit cell and by either one or two CO molecules per unit cell.[72] In the latter case, for which the unit cell contains one oxygen atom and two CO molecules, the CO saturation coverage should amount to 0.5 per surface Pd atom, which is in good agreements with the experimentally measured value ~0.51.

On O/Pd(111), the initial heat of CO adsorption amounts to 104 ± 4 kJ mol^{-1}, which is ~45 kJ mol^{-1} lower than the CO adsorption energy on the pristine Pd(111) surface. The initial CO adsorption heat on Pd nanoparticles precovered with oxygen reaches 95 ± 2 kJ mol^{-1}. This value is ~39 kJ mol^{-1} lower than the initial heat of CO adsorption on the clean Pd nanoparticles. Interestingly, both O-presaturated surfaces show a similar decrease of the CO adsorption energy by ~40–45 kJ mol^{-1}. Moreover, the same energy difference (~40 kJ mol^{-1}) in CO adsorption heat was observed over the whole range of CO surface coverages on both surfaces (data not show).

Two major observations can be made from the comparison of clean *vs.* O-precovered Pd surfaces with respect to the CO adsorption energies. First, the presence of a monolayer of co-adsorbed oxygen atoms lowers the CO binding energy by about 40–45 kJ mol^{-1} both on the single crystal surface and on Pd nanoparticles. This value can be considered as a measure for the repulsive interaction between oxygen and CO on Pd. Second, the difference between CO binding energies on Pd(111) and Pd nanoparticles of about 10–15 kJ mol^{-1} remains preserved even on the O-covered surfaces. Previously, the decreasing CO adsorption energy with decreasing particle size on clean Pd particles was attributed primarily to the contraction of the Pd lattice in small clusters. The presented data demonstrate that the same trend is valid also for Pd surfaces covered with oxygen with approximately the same magnitude.

Conclusions

In conclusion, we investigated the interaction of CO and O_2 molecules with well-defined Pd nanoclusters and with the extended Pd(111) surface by a direct calorimetric method. The main focus of this study lies in a detailed understanding of how a nanometer scale confinement of matter affects the binding strength of gaseous adsorbates relevant to CO oxidation.

CO and oxygen adsorption were investigated both on clean and O-precovered Pd nanoparticles and Pd(111) and corresponding sticking coefficients and adsorption energies were determined as a function of adsorbate coverages.

The CO adsorption kinetics on Pd nanoparticles investigated by the King–Well method show a strong enhancement of the adsorbate flux onto Pd clusters due to a "capture zone" effect, which involves weak trapping of the adsorbates on the support and diffusion to the metal particles. The CO adsorption rate on nanoparticles was estimated to be enhanced by factor of 1.4–1.9 depending on the assumptions on the initial sticking coefficient on metallic Pd. For oxygen adsorption, the "capture zone effect" was found to also play a role; however, its exact quantification was difficult because of possibly higher activity of Pd nanoparticles towards dissociative O_2 adsorption as compared to Pd(111).

The initial binding energy of carbon monoxide was found to be lower on Pd nanoparticles than on Pd(111) (134 *vs.* 149 kJ mol^{-1}, correspondingly) despite the high fraction of low-coordinated surface sites present on nanoclusters. This observation can be rationalized as a consequence of Pd lattice contraction in small particles leading to weakening of chemisorptive interaction. Additionally, a reduced polarizability of small Pd nanoparticles can result in a reduction of van der Waals attraction. On the O-precovered Pd surfaces, the CO binding energy was found to be reduced by about 40–45 kJ mol^{-1} as compared to the corresponding pristine Pd surfaces in the full range of CO coverages. Also in the presence of a monolayer of oxygen, CO binds weaker on Pd nanoclusters than on Pd(111) by about 10–15 kJ mol^{-1}. This result suggests that the strain effect observed for pristine Pd nanoclusters remains preserved also on the particles pre-covered with adsorbates, particularly oxygen.

Table 1 Summary of the adsorption energies of the CO and oxygen adsorbates on the clean O-precovered Pd surfaces obtained in this study

	Adsorption enthalpy, kJ mol^{-1} (low coverage → quasi saturation[a])	
	Pd(111)	Pd nanoparticles (~4 nm)/Fe_3O_4/Pt(111)
CO on pristine Pd, 300 K	149 ± 4 → 75	134 ± 4 → 90
O_2 on pristine Pd (per O_2 molecule), 300 K	205 ± 7 → 100	280 ± 13 → 100
CO on O (1 ML)/Pd, 100 K	104 ± 4 → 30	94 ± 2 → 30

[a] Note that the absolute accuracy of the enthalpy values in the quasi saturation regime is lower than for the lowest adsorbate coverage because of the experimental difficulties in determining very low sticking coefficients.

The measured initial oxygen adsorption heat on Pd(111) amounts to 205 ± 7 kJ mol^{-1}. On Pd nanoparticles, this values increases by ~75 kJ mol^{-1}; this energy can be attributed to strong oxygen binding at the low coordinated adsorption sites of Pd nanoparticles such as edges as corners, which was also confirmed by spectroscopic data. The unexpectedly strong binding energy of oxygen at the particles edges exceeds all literature values of oxygen adsorption energies at stepped single crystal surfaces. Apparently, the local adsorption environment of Pd–O bond plays a very important role in determining the binding strength in this adsorption system. This result is in a sharp contrast to the CO–Pd case, where the presence of the low-coordinated surface sites on a Pd nanoparticle was observed to not result in stronger CO–Pd binding energy. Instead, weakening of CO interaction energy with Pd nanoparticles was detected, which can be most likely attributed to the contraction of the Pd lattice. Both Pd surfaces exhibit very strong coverage dependence of O binding energy covering the range up to 180 kJ mol^{-1}.

In summary, the reduced dimensions of the Pd substrate can affect the binding strength of the adsorbates involved in CO oxidation in two principle ways: (i) *via* the change of the local adsorption environment that can result *e.g.* in stronger adsorbate bonding *e.g.* at the particle edges and (ii) *via* contraction of the Pd lattice in small clusters and a concomitant weakening of chemisorptive interaction. The latter effect is expected to play a role not only for CO as shown in this study but also for other adsorbates (provided that the local adsorption environment remains preserved). The presented experimental data (summarized in Table 1) provide important benchmarks for upcoming theoretical calculation.

Acknowledgements

Support by the Fonds der Chemischen Industrie is gratefully acknowledged. The authors thank Hans-Joachim Freund, Charles T. Campbell (UW) and Beatriz Roldan (UCF) for valuable discussions.

References

1 G. Ertl, H. Knoezinger and J. Weitkamp, in *Handbook of Heterogeneous Catalysis*, ed. G. Ertl, H. Knoezinger and J. Weitkamp, VCH, Weinheim, 1997.
2 J. M. Thomas and W. J. Thomas, *Principle and Practice of Heterogeneous Catalysis*, VCH, Weinheim, 1997.
3 T. Engel and G. Ertl, *Adv. Catal.*, 1979, **28**, 41.
4 S. M. McClure and D. W. Goodman, *Chem. Phys. Lett.*, 2009, **469**, 1.
5 J. Libuda and H.-J. Freund, *Surf. Sci. Rep.*, 2005, **57**, 157.
6 J. Wintterlin, S. Völkening, T. V. W. Janssens, T. Zambelli and G. Ertl, *Science*, 1997, **278**, 1931.

7 C. R. Henry, *Surf. Sci. Rep.*, 1998, **31**, 231.
8 I. Stará and V. Matolín, *Surf. Sci.*, 1994, **313**, 99.
9 G. Zheng and E. I. Altman, *Surf. Sci.*, 2002, **504**, 253.
10 H. Conrad, G. Ertl, J. Küppers and E. E. Latta, *Surf. Sci.*, 1977, **65**, 245.
11 R. Westerström, J. Gustafson, A. Resta, A. Mikkelsen, J. N. Andersen, E. Lundgren, N. Seriani, F. Mittendorfer, M. Schmidt, J. Klikovits, P. Varga, M. D. Ackermann, J. W. M. Frenken, N. Kasper and A. Stierle, *Phys. Rev. B*, 2007, **76**, 155410.
12 F. P. Leisenberger, G. Koller, M. Sock, S. Surnev, M. G. Ramsey, F. P. Netzer, B. Klötzer and K. Hayek, *Surf. Sci.*, 2000, **445**, 380.
13 G. Zheng and E. Altman, *Surf. Sci.*, 2000, **462**, 151.
14 A. Vlad, A. Stierle, R. Westerström, S. Blomberg, A. Mikkelsen and E. Lundgren, *Phys. Rev. B*, 2012, **86**, 35407.
15 B. Klötzer, K. Hayek, C. Konvicka, E. Lundgren and P. Varga, *Surf. Sci.*, 2001, **482–485**, 237.
16 P. Nolte, A. Stierle, N. Kasper, N. Y. Jin-Phillipp, N. Jeutter and H. Dosch, *Nano Lett.*, 2011, **11**, 4697.
17 R. Westerström, M. E. Messing, S. Blomberg, A. Hellman, H. Grönbeck, J. Gustafson, N. M. Martin, O. Balmes, R. van Rijn, J. N. Andersen, K. Deppert, H. Bluhm, Z. Liu, M. E. Grass, M. Hävecker and E. Lundgren, *Phys. Rev. B*, 2011, **83**, 115440.
18 J. Han, G. Zhu, D. Y. Zemlyanov and F. H. Ribeiro, *J. Catal.*, 2004, **225**, 7.
19 E. Lundgren, G. Kresse, C. Klein, M. Borg, J. N. Andersen, M. de Santis, Y. Gauthier, C. Konvicka, M. Schmidt and P. Varga, *Phys. Rev. Lett.*, 2002, **88**, 246103.
20 T. Schalow, M. Laurin, B. Brandt, S. Schauermann, S. Guimond, H. Kuhlenbeck, D. E. Starr, S. K. Shaikhutdinov, J. Libuda and H.-J. Freund, *Angew. Chem., Int. Ed.*, 2005, **44**, 7601.
21 W. A. Brown, R. Kose and D. A. King, *Chem. Rev.*, 1998, **98**, 797.
22 J. Stuckless, N. Frei and C. T. Campbell, *Rev. Sci. Instrum.*, 1998, **69**, 2427.
23 C. T. Campbell and O. Lytken, *Surf. Sci.*, 2009, **603**, 1365.
24 J.-H. Fischer, J. Hartmann, J. A. Farmer, J. M. Flores-Camacho, C. T. Campbell, S. Schauermann and H.-J. Freund, *Rev. Sci. Instrum.*, 2011, **82**, 24102.
25 D. King and M. Wells, *Surf. Sci.*, 1972, **29**, 454.
26 T. Schalow, B. Brandt, D. E. Starr, M. Laurin, S. K. Shaikhutdinov, S. Schauermann, J. Libuda and H.-J. Freund, *Phys. Chem. Chem. Phys.*, 2007, **9**, 1347.
27 T. Schalow, B. Brandt, D. E. Starr, M. Laurin, S. Schauermann, S. K. Shaikhutdinov, J. Libuda and H.-J. Freund, *Catal. Lett.*, 2006, **107**, 189.
28 C. Lemire, R. Meyer, V. Henrich, S. K. Shaikhutdinov and H.-J. Freund, *Surf. Sci.*, 2004, **572**, 103.
29 T. Mitsui, M. K. Rose, E. Fomin, D. F. Ogletree and M. Salmeron, *Phys. Rev. Lett.*, 2005, **94**, 036101.
30 A. M. Bradshaw and F. M. Hoffmann, *Surf. Sci.*, 1978, **72**, 513.
31 J. Szanyj, W. K. Kuhn and D. W. Goodman, *J. Vac. Sci. Technol., A*, 1993, **11**, 1969.
32 S. Surnev, M. Sock, M. G. Ramsey, F. P. Netzer, M. Wiklund, M. Borg and J. N. Andersen, *Surf. Sci.*, 2000, **470**, 171.
33 T. Gießel, O. Schaff, C. J. Hirschmugl, V. Fernandez, K.-M. Schindler, A. Theobald, S. Bao, R. Lindsay, W. Berndt, A. M. Bradshaw, C. Baddeley, A. F. Lee, R. M. Lambert and D. P. Woodruff, *Surf. Sci.*, 1998, **406**, 90.
34 H. Conrad, G. Ertl, J. Kocha and E. E. Latta, *Surf. Sci.*, 1974, **43**, 462.
35 T. Engel, *J. Chem. Phys.*, 1978, **69**, 373.
36 A. Ortega, F. M. Hoffmann and A. M. Bradshaw, *Surf. Sci.*, 1982, **119**, 79.
37 K. Tsu and M. Boudart, *2nd Actes du Congr. Int. Cat. (Technip, Paris)*, 1961, **1**, 593.
38 Y. Kim and M. Boudart, *Langmuir*, 1991, **7**, 2999.
39 E. Gillet, S. Channakhone, V. Matolin and M. Gillet, *Surf. Sci.*, 1985, **152–153**, 603.
40 V. Matolin and E. Gillet, *Surf. Sci.*, 1986, **166**, L115.
41 M. Bowker, P. Stone, R. Bennett and N. Perkins, *Surf. Sci.*, 2002, **497**, 155.
42 H. Conrad, G. Ertl, J. Koch and E. E. Latta, *Surf. Sci.*, 1974, **43**, 462.
43 G. Ertl and J. Koch, *Z. Naturforsch.*, 1970, **25a**, 1906.
44 R. D. Ramsier, K.-W. Lee and J. T. Yates, Jr., *Surf. Sci.*, 1995, **322**, 243.
45 T. Engel, *J. Chem. Phys.*, 1978, **69**, 373.
46 J.-H. Fischer-Wolfarth, J. A. Farmer, J. M. Flores-Camacho, A. Genest, I. V. Yudanov, N. Rösch, C. T. Campbell, S. Schauermann and H.-J. Freund, *Phys. Rev. B*, 2010, **81**, 241416.
47 I. V. Yudanov, R. Sahnoun, K. M. Neyman, N. Rösch, J. Hoffmann, S. Schauermann, V. Johánek, H. Unterhalt, G. Rupprechter, J. Libuda and H.-J. Freund, *J. Phys. Chem. B*, 2003, **107**, 255.
48 C. T. Campbell, G. Ertl, H. Kuipers and J. Segner, *Surf. Sci.*, 1981, **107**, 207.

49 S. A. Nepijko, M. Klimenkov, M. Adelt, H. Kuhlenbeck, R. Schlögl and H.-J. Freund, *Langmuir*, 1999, **15**, 5309.
50 R. Lamber, S. Wetjen and N. I. Jaeger, *Phys. Rev. B*, 1995, **51**, 10968.
51 S. Krüger, S. Vent, F. Nörmann, M. Staufer and N. Rösch, *J. Chem. Phys.*, 2001, **115**, 2082.
52 P. Nava, M. Sierka and R. Ahlrichs, *Phys. Chem. Chem. Phys.*, 2003, **5**, 3372.
53 O. Häberlen, S.-C. Chung, S. Krüger and N. Rösch, *J. Chem. Phys.*, 1997, **106**, 5189.
54 I. V. Yudanov, R. Sahnoun, K. M. Neyman and N. Rösch, *J. Chem. Phys.*, 2002, **117**, 9887.
55 I. V. Yudanov, M. Metzner, A. Genest and N. Rösch, *J. Phys. Chem. C*, 2008, **112**, 20269.
56 E. Shustorovich and H. Sellers, *Surf. Sci. Rep.*, 1998, **31**, 1.
57 R. A. van Santen and G. J. Kramer, *Chem. Rev.*, 1995, **95**, 637.
58 B. Hammer, Y. Morikawa and J. K. Nørskov, *Phys. Rev. Lett.*, 1996, **76**, 2141.
59 S. Sandel, J. Libuda, P. Brühwiler, S. Andersson, A. J. Maxwell, M. Bäumer, N. Mårtensson and H.-J. Freund, *J. Vac. Sci. Technol., A*, 1996, **14**, 1546.
60 K. Watanabe, Y. Matsumoto, M. Kampling, K. Al-Shamery and H.-J. Freund, *Angew. Chem., Int. Ed.*, 1999, **38**, 2192.
61 D. Mulugeta, K. H. Kim, K. Watanabe, D. Menzel and H.-J. Freund, *Phys. Rev. Lett.*, 2008, **101**, 146103.
62 To be published.
63 P. W. Davies and R. M. Lambert, *Surf. Sci.*, 1981, **110**, 227.
64 K. Hµjrup Hansen, Ž. Šljivančanin, E. Lęgsgaard, F. Besenbacher and I. Steinsgaard, *Surf. Sci.*, 2002, **505**, 25.
65 K. Wolter, O. Seiferth, H. Kuhlenbeck, M. Bäumer and H.-J. Freund, *Surf. Sci.*, 1998, **399**, 190.
66 M. Peter, J. M. Flores Camacho, S. Adamovsky, L. K. Ono, K.-H. Dostert, C. P. O'Brien, B. Roldan Cuenya, S. Schauermann and H.-J. Freund, *Angew. Chem., Int. Ed.*, 2013, DOI: 10.1002/anie.201209476.
67 P. Nolte, A. Stierle, N. Kasper, N. Y. Jin-Phillipp, N. Jeutter and H. Dosch, *Nano Lett.*, 2011, **11**, 4697.
68 T. Gießel, O. Schaff, C. J. Hirschmugl, V. Fernandez, K.-M. Schindler, A. Theobald, S. Bao, R. Lindsay, W. Berndt, A. M. Bradshaw, C. Baddeley, A. F. Lee, R. M. Lambert and D. P. Woodruff, *Surf. Sci.*, 1998, **406**, 90.
69 D. Loffreda, D. Simon and P. Sautet, *Surf. Sci.*, 1999, **425**, 68.
70 L. Surnev, M. Sock, M. G. Ramsey, F. P. Netzer, M. Wiklund, A. Borg and J. N. Andersen, *Surf. Sci.*, 2000, **470**, 171.
71 M. K. Rose, T. Mitsui, J. C. Dunphy, A. Borg, D. F. Ogletree, M. Salmeron and P. Sautet, *Surf. Sci.*, 2002, **512**, 48.
72 J. Méndez, S. H. Kim, J. Cerdá, J. Wintterlin and G. Ertl, *Phys. Rev. B*, 2005, **71**, 085409.

